Vietnam Journal of Science and Technology ***60*** *(2) (2022) 216-224*

doi:10.15625/2525-2518/16266

BREAKDOWN CHARACTERISTICS OF GLASS FIBER REINFORCED EPOXY FOR TERMINATION OF HIGH TEMPERATURE SUPERCONDUCTING CABLE

Nguyen Van Dung*, Le Vinh Truong

Cantho University, Can Tho City, 3/2 Street, Ninh Kieu District, Viet Nam

*Emails: *nvdung@ctu.edu.vn*

Received: 7 July 2021; Accepted for publication: 4 October 2021

Abstract. A study on the effect of the physical states of nitrogen on the breakdown properties of glass fiber reinforced epoxy was carried out. Surface breakdown and volume breakdown of glass fiber reinforced epoxy in nitrogen gas, cryogenic nitrogen gas and liquid nitrogen under AC voltages were investigated. In addition, breakdown strength-time to breakdown characteristics of glass fiber reinforced epoxy in these insulating media were also examined. The experimental data showed that surface breakdown strength and volume breakdown strength of glass fiber reinforced epoxy were significantly dependent on surrounding media, and similar results were obtained with breakdown strength-time to breakdown experiments. Glass fiber reinforced epoxy has the surface breakdown strength of 2.5 - 4.5 kV/mm, 8 - 16 kV/mm and 15 - 25 kV/mm when immersed in nitrogen gas, cryogenic nitrogen gas and liquid nitrogen, respectively. Similarly, the volume breakdown strength of glass fiber reinforced epoxy was determined to be about 48 kV/mm in nitrogen gas, 49 kV/mm in cryogenic nitrogen gas and 40 kV/mm in liquid nitrogen. For surface breakdown test, the lifetime index of glass fiber reinforced epoxy reached the highest value in nitrogen gas (55.6) and the lowest value in liquid nitrogen (43.5). For puncture breakdown test, glass fiber reinforced epoxy has the lifetime index of 47.6, 41.7 and 38.5 when immersed in nitrogen gas, cryogenic nitrogen gas and liquid nitrogen.

Keywords: Breakdown strength, glass fiber, epoxy, superconducting, termination.

Classification numbers: 2.3.1, 2.8.3.

1. INTRODUCTION

The discovery of the so-called high temperature superconductor (HTS) operating at temperatures above 77 K in 1987 renewed interest in superconducting power generation and transmission. Especially, HTS cable promises to transmit a large capacity of electric power with lower voltage and in a compact size [1 - 2]. Cable termination is one of the essential components for an HTS cable system because it is used to connect an HTS power cable to a generator or a transformer at room temperature. The termination must span a wide range of temperature, i.e. from 77 K to 300 K. Thus, the combination of liquid nitrogen with nitrogen gas and solid polymer was used for electrical insulation of the termination [3, 4]. With this hybrid insulation

system, there is the existence of discharges inside the volume of solid polymers as well as on its surfaces. Glass fiber reinforced epoxy (GFRP) has been studied for using as body insulation in HTS termination [5 - 8]. It was obtained that GFRP had a similar breakdown voltage but higher tensile strength than other solid insulators, i.e. silicone rubber, ethylene propylene diene monomer, aromatic polyamide and polytetrafluoroethylene, at cryogenic temperature [5]. Thus, GFRP has been selected as an insulator for HTS termination in this study. Surface discharges of GFRP in various physical states of nitrogen for an HTS termination were presented in previous studies [7, 8], where there is, however, still a lack of data on puncture breakdown of GFRP, breakdown strength-time relationship and breakdown characteristics of GFRP for insulation design of the HTS termination. Therefore, an investigation of the influence of different states of nitrogen on breakdown characteristics of GFRP for providing a better insight in this field of study is essential. Furthermore, there are currently no studies on insulation for HTS termination or other HTS devices in Viet Nam. However, we predict that HTS equipment will be investigated in the near future in Viet Nam due to the need for higher electric power transmission at lower voltage. Thus, this study will establish a basis for further researches.

2. MATERIALS AND METHODS

2.1. Experimental setup

Figure 1 shows the experimental setup for determining the surface breakdown strength of glass fiber reinforced epoxy (GFRP) in nitrogen gas (GN_2), cryogenic nitrogen gas (CGN_2), and liquid nitrogen (LN_2) with changing the electrode gap (L) from 1.0 cm to 5.0 cm. GFRP was produced from FR4 epoxy containing about 60 % glass fiber (E-glass) and 40 % epoxy resin by weight. The GFRP sheets originating from China were supplied by a local company, and had the technical data shown in Table 1. In the case of CGN_2, the GFRP sheet was placed about 10 mm above LN_2 surface. For the LN_2 case, the whole electrode system and the GFRP sample was immersed in LN_2 while GN_2 occupied the whole volume of the cryostat vessel for the GN_2 case. The pressure of GN_2 and CGN_2 is 1 atm. The experimental setup for measuring the puncture breakdown strength of GFRP sample was similar to that of the surface breakdown strength case shown in Fig. 1.

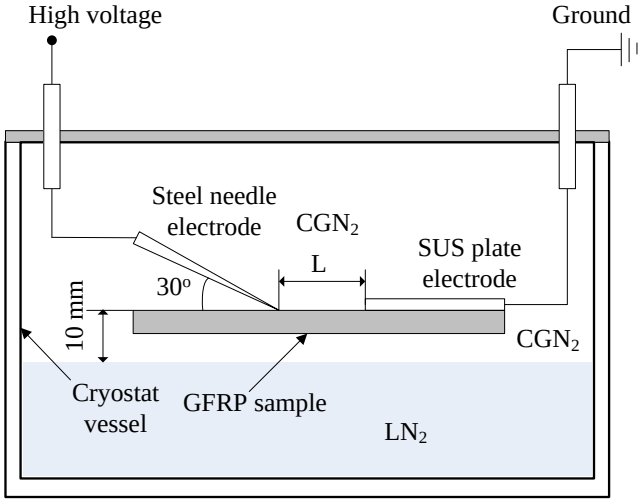

Figure 1. Experimental setup for surface breakdown test of GFRP samples.

Table 1. Technical data of GFRP sheet.

No	Parameters	Unit	Value
1	Density	g/cm^3	2 - 2.1
2	Water absorption	%	≤ 0.15
3	Tensile strength at yield	MPa	≥ 240
4	Max. service temperature	^oC	280
5	Volume resistivity	Ω.cm	5.10^9 - 5.10^{11}
6	Surface resistivity	Ω	5.10^{10} - 5.10^{12}
7	Dielectric constant	-	5.5

However, the needle-plate electrode system was replaced with a sphere-plane electrode system (Fig. 2). The experiments were also performed with GFRP samples in GN_2, CGN_2 and LN_2. GFRP samples with a thickness of 0.5 mm were used, and for the case of LN_2, the thickness of GFRP samples was varied from 0.5 mm to 2.0 mm. To observe the erosion of GFRP after puncture breakdown, the surface image of a typical GFRP sample with a thickness of 0.5 mm after breakdown was captured with a digital camera named Fujifilm FinePix JZ300 (10x optical zoom, 16 megapixel).

For determining the breakdown strength-time (*E-t*) characteristics of GFRP samples, the electrode systems shown in Fig. 1 and Fig. 2 were used for surface and puncture discharges, respectively.

All experiments were performed under AC voltages, and an AC dielectric strength test set (50/60 Hz, 100 kV, 1 kVA) made by Kyonan Electric CO., LTD was used to exert high voltage to the electrode system.

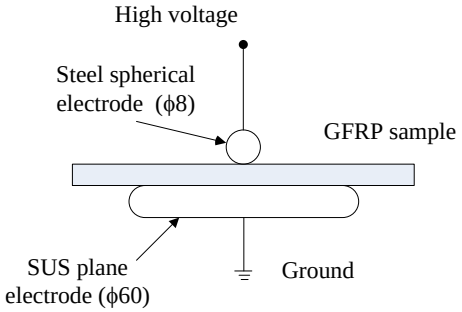

Figure 2. Electrode system for puncture breakdown test of GFRP sample.

2.2. Method and procedure

The breakdown test was carried out according to ASTM D149 [9]. The test samples were subjected to a slow AC ramp (1 kV/s) until breakdown [9]. The test was repeated 6 times for each value of electrode gap and thickness of GFRP samples to obtain an average value of surface and puncture breakdown strengths. In order to investigate *E-t* characteristics, the average breakdown strength (E_{ave}) was first determined from six breakdown tests, and then the time to breakdown was measured with varying the applied field strength from about 60 % to 100 % of E_{ave}. The breakdown test was performed to measure the short-term withstand strength of GFRP samples while *E-t* test was used to determine the long-term withstand strength of insulating

samples. The short-term withstand strength represents the intrinsic strength of insulating materials while the long-term withstand strength shows the strength of materials under ageing when subjected to voltage for a long time.

3. RESULTS AND DISCUSSION

3.1. Surface breakdown strength

The surface breakdown strength (E_F) of GFRP samples in CGN_2, GN_2, and LN_2 was found to decrease significantly with increasing electrode gap, d, as seen in Fig. 3. It is clear that the E_F of the GFRP samples strongly depends on medium surrounding the samples. The reason is that surrounding medium plays a significant role in the growth of electron avalanches near insulating surfaces and discharge trajectory at flashover, which partially governs the surface breakdown strength [10-12]. At first, the E_F declines quickly and then starts to level off when the gap distance exceeds the value of 5.0 cm. This is because the surface discharges are more controlled by partial discharges at the tip of high voltage electrode for short gaps, but the surface conditions will play a dominant role for longer gaps [13]. The E_F of the GFRP samples in LN_2 reaches the highest value while the lowest value is obtained for the case of GFRP in GN_2. A similar result was reported by other researchers [14, 15]. This can be explained by the fact that the surface discharges will start with partial discharges (PD) at the tip of the needle electrode and then the discharges creep on the GFRP surface in a zigzag path. This is because GFRP has higher permittivity than GN_2, CGN_2 or LN_2, leading to more charge accumulation on the GFRP surface [13]. Thus, this results in discharges on the GFRP surface instead of in GN_2, CGN_2 or LN_2. In addition, the PD at the needle tip significantly depends on its surrounding media, and PD was observed to occur at a higher voltage value in LN_2 than in GN_2 and CGN_2 [4]. For comparison, the breakdown strength of the gap containing only LN_2 is also presented in Fig. 3. It was observed that the existence of a GFRP sheet reduced the breakdown strength of LN_2 by about 20 %. For the sake of clarity, the breakdown strength of GN_2 and CGN_2 is not shown in Fig. 3. However, the results obtained in these cases are similar to the case of LN_2.

3.2. Puncture breakdown strength

The effect of surrounding medium on the puncture breakdown strength (E_{BD}) of the GFRP samples with a thickness of 0.5 mm is shown in Fig. 4. In this figure, the E_{BD} takes the values of 42.2 kV/mm, 48.2 kV/mm and 49.4 kV/mm for the cases of LN_2 (77 K), GN_2 (300 K) and CGN_2 (90 K), respectively. This demonstrates that the E_{BD} of GFRP samples is more dependent on the state of the insulating medium (liquid or gas) than the temperature of the insulating medium (90 K or 300 K). This result can be explained by the formation of micro-cracks resulting from thermal contraction when the temperature of GFRP samples is suddenly reduced by immersing them in LN_2. In addition, micro-bubbles in LN_2 at liquid wedge between the sphere electrode and sample surface could promote partial discharges, leading to surface erosion of the GFRP sample as shown in Fig. 5a. This considerably reduces the E_{BD} of GFRP samples. Fig. 5a was produced by capturing the image of the surface of a GFRP sample after a breakdown test at 40.6 kV/mm with a digital camera. The puncture breakdown of GFRP samples will start with the occurrence of partial discharges in the gas or liquid wedge (Fig. 5b). This is because dielectric constants of GN_2 ($\varepsilon_r \sim 1.0$), CGN_2 ($\varepsilon_r \sim 1.0$) and LN_2 ($\varepsilon_r \sim 1.4$) are lower than that of GFRP ($\varepsilon_r \sim 5.5$). Therefore, the electric field in the gas or liquid wedge is high enough to trigger the partial discharges. These discharges cause serious damage of the GFRP sample surface by the

bombardment of energetic electrons and ions. Moreover, ultraviolet, heat and shockwave can further erode the GFRP sample surface. Simultaneously, partial discharges may take place in voids or air bubbles inside the sample, which rapidly degrades the sample and ultimately leads to puncture breakdown.

Figure 6 shows the correlation between the E_{BD} and thickness, d, of GFRP samples in LN_2. It was observed that the E_{BD} decreases nonlinearly with d, and the influence of d on the E_{BD} decreases with an increase in thickness. This result is in good agreement with those reported for other materials in LN_2 [2]. The reason may be due to the so-called "thickness effect", which means an increase in thickness will raise the number of voids, air bubbles, micro-cracks, etc. inside GFRP samples. This results in partial discharges that reduce the E_{BD}. However, when the thickness increases to a critical value, the breakdown will not depend on the number of voids or air bubbles inside the sample since there is sufficient number of voids or air bubbles for partial discharges to occur. This results in leveling off the E_{BD} at high thickness values. For comparison, Fig. 6 also shows the E_{BD} of LN_2. It was obtained that the E_{BD} of GFRP samples in LN_2 is about 30 % higher than that of LN_2 gap only. This is because the existence of a GFRP sheet will stop the streamer propagation in the electrode gap [16], i.e. prevent the breakdown process.

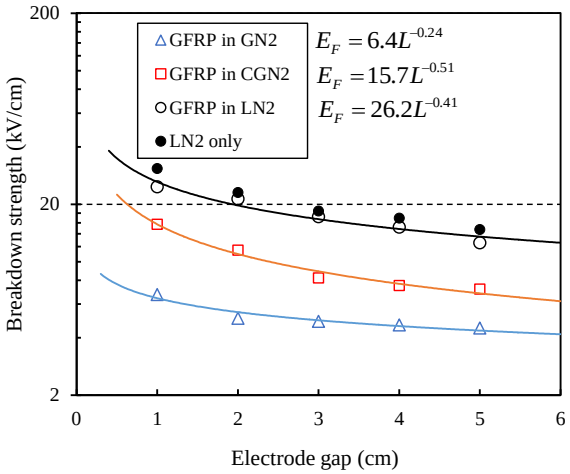

Figure 3. Surface breakdown strength versus electrode gap of GFRP sample.

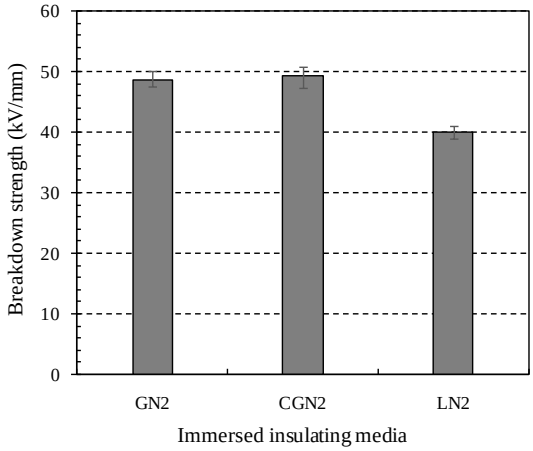

Figure 4. The volume breakdown strength of GFRP versus insulating media (d = 0.5 mm).

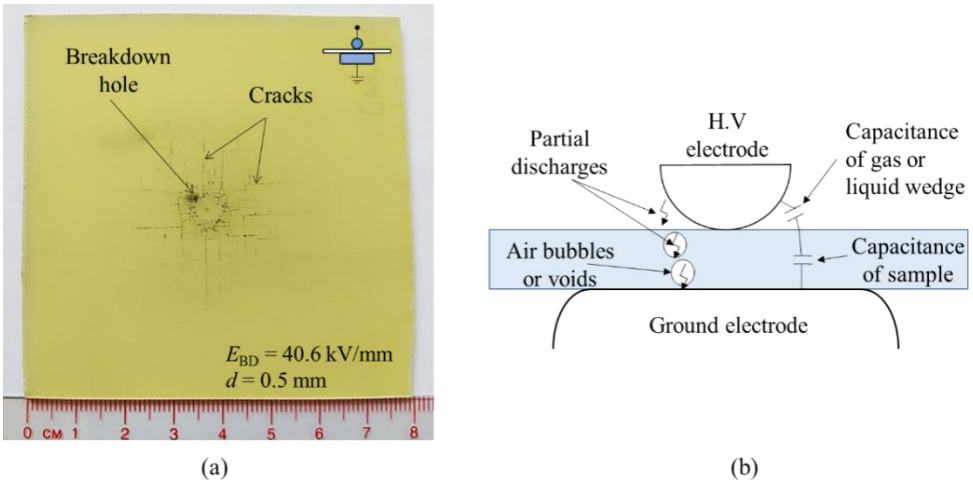

Figure 5. GFRP sample in LN_2 after puncture breakdown: erosion of sample (a) and breakdown model (b).

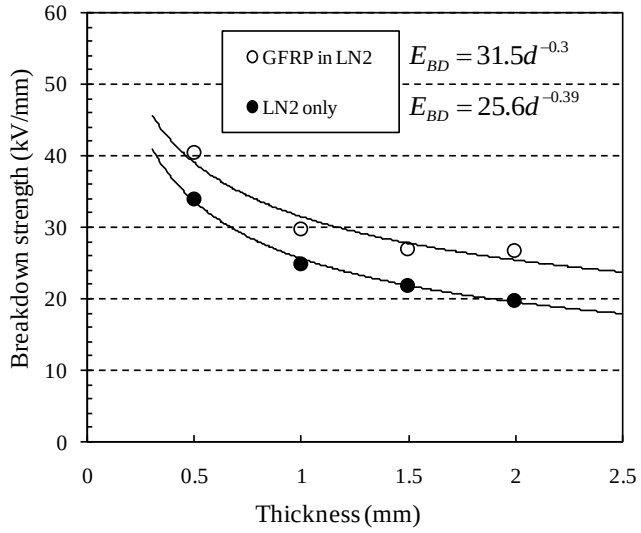

Figure 6. Correlation between the puncture breakdown strength and thickness of GFRP samples in LN_2.

3.3. *E-t* characteristics

Figure 7 shows the *E-t* characteristics of GFRP in GN_2, CGN_2 and LN_2 for the case of surface discharges. The electrode gap of 5.0 cm was used for investigating the *E-t.* This is because the decline rate in E_F starts to decrease around this gap value, as seen in Fig. 3. It was observed that an increase in the field stress, *E*, results in a significant reduction in time to breakdown, *t*. The correlation between *E* and *t* follows a power law expressed by equation (1) [2]. This is in agreement with those reported for other insulators in LN_2 [2]. Both constant *A* and lifetime index *n* change with insulating medium in which GFRP samples are immersed. The GFRP samples in LN_2 show the highest value of *A*, but the *n* of this case takes the minimum value. This indicates that although the GFRP samples have a higher dielectric strength in LN_2 than in CGN_2 and GN_2 (Fig. 3), the degradation rate of the GFRP samples in LN_2 due to surface discharges is the highest compared to other cases. This is because of higher applied field stress as well as the effect of thermal contraction on GFRP samples in LN_2 as explained above.

$$E = At^{-1/n}. \quad (1)$$

Figure 8 shows the *E-t* characteristics of GFRP samples for puncture discharges. It was also observed that the immersing medium significantly affects the *E-t* of GFRP samples. Similar to the case of surface discharges, the lifetime index *n* was seen to decrease sequentially from GN_2, CGN_2 to LN_2 (47.6 for GN_2; 41.7 for CGN_2; and 38.5 for LN_2). This confirms that GFRP samples are degraded more rapidly in LN_2 than in GN_2 and CGN_2. In addition, the *E-t* of GFRP samples was also affected by their thickness. Both constant *A* and lifetime index *n* are higher for thinner sheet of GFRP in LN_2. The reason is that increasing the thickness will increase the number of impurities, voids and air bubbles in the bulk of GFRP samples leading to lower values of the breakdown strength and the lifetime index. For the sake of clarity, the effect of thickness on *E-t* of GFRP samples in GN_2 and CGN_2 is not shown in Fig. 8, but it was observed that similar results to the LN_2 case were also obtained.

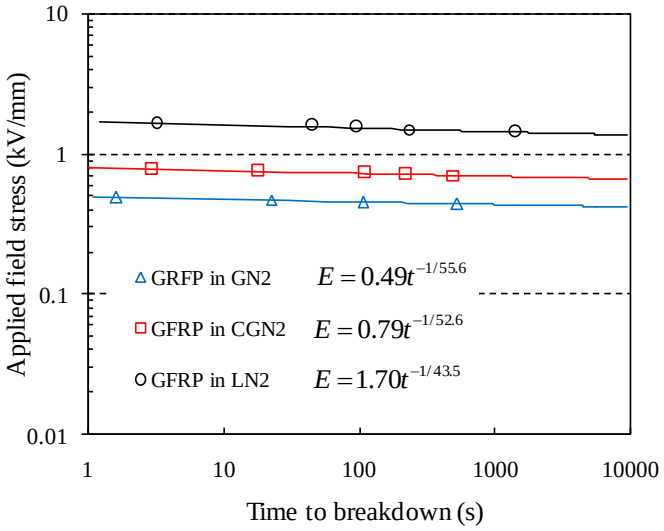

Figure 7. E-t characteristics of GFRP samples for surface discharge case.

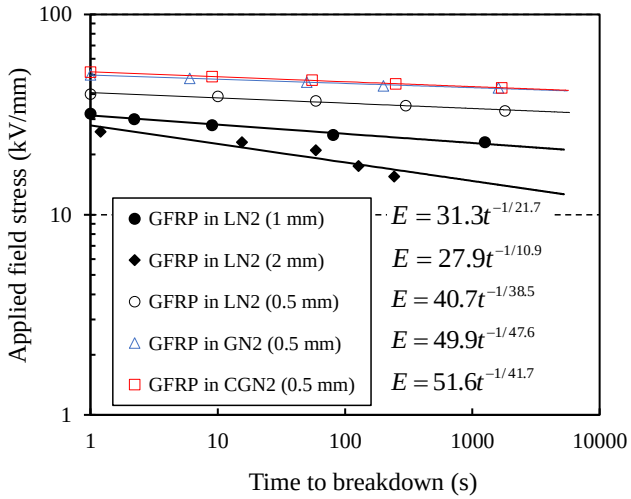

Figure 8. E-t characteristics of GFRP samples for puncture discharge case.

4. CONCLUSIONS

A basic study on breakdown characteristics of GFRP samples for designing HTS termination was performed. The surface and puncture breakdown strengths of GFRP samples considerably depend on the discharge length and immersing insulating media. For surface discharges, the highest strength of GFRP samples was obtained in LN_2 case (15-25 kV/cm). However, it is aware that for long-term discharges, GFRP samples are more aged under LN_2 compared to GN_2 and CGN_2 (n = 43.5 for LN_2; 55.6 for GN_2; and 52.6 for CGN_2). For the puncture breakdown, the strength of GFRP samples reached the lowest value in the LN_2 case (~40 kV/mm at a thickness of 0.5 mm) and had a tendency to decrease with increasing the thickness, and the lifetime index n reached the highest value for the GN_2 case (47.6) and the lowest value for the LN_2 case (38.5). In addition, the n decreased with increasing the thickness of GFRP samples in LN_2 (38.5 at 0.5 mm; 21.7 at 1.0 mm and 10.9 at 2.0 mm). Future work will be done with impulse breakdown and partial discharges of GFRP samples.

CRediT authorship contribution statement. Nguyen Van Dung: Methodology, Data analysis, Writing paper. Le Vinh Truong: Experiments.

Declaration of competing interest. The authors declare that they have no known competing financial interests or personal relationships that could have appeared to influence the work reported in this paper.

REFERENCES

1. Politano D., Sjostrom M., Schnyder G. and Rhyner J. - Technical and economical assessment of HTS cables, IEEE Trans. Applied Superconductivity **11** (1) (2001) 2477-2480. https://doi.org/10.1109/77.920366.
2. Bulinski A. and Densley J. - High voltage insulation for power cables utilizing high temperature superconductivity, IEEE Electrical Insulation Magazine **15** (2) (1999) 14-22. https://doi.org/10.1109/57.753927.
3. Kwag D. S., Cheon H. G., Choi J. H., Kim H. J., Cho J. W., Yun M. S. and Kim S. H. - The electrical insulation characteristics for a HTS cable termination, IEEE Trans. Applied Superconductivity **16** (2) (2006) 1618-1621. https://doi.org/10.1109/TASC.2006.870519.
4. Minami Y., Nagaya S., Suzawa C., Chigusa S., Isojima S., Hayakawa N. and Okubo H. - Discharge characteristics on the surface of solid insulator in liquid nitrogen, Proceeding of ICDL, Japan, 1999, pp. 474-478.
5. Kim W. J., Shin H. S. and Kim S. H. - A Study on the body insulators for the bushing for HTS devices at cryogenic temperature, Physics Procedia **45** (2013) 313-316. http://dx.doi.org/10.1016/j.phpro.2013.05.030.
6. Ren L., Tang Y., Shi J. and Jiao F. - Design of a termination for the hts power cable, IEEE Trans. Applied Superconductivity **22** (3) (2012) 5800504.

   https://doi.org/10.1109/TASC.2012.2191482.
7. Kwag D. S., Cheon H. G., Choi J. H., Kim H. J., Cho J. W. and Kim S. H. - Research on the insulation design of a 154 kV class HTS power cable and termination, IEEE Trans. Applied Superconductivity **17** (2) (2007) 1738-1742.

   https://doi.org/10.1109/TASC.2007.899211.

8. Kim H. J., Kim W. J. and Kim S. H. - A study on the insulation of the termination for HTS cable in liquid nitrogen, J. Supercond. Nov. Magn. **28** (2) (2015) 615-618. http://dx.doi.org/10.1007/s10948-014-2731-9.
9. ASTM Standard D149-97a, Standard test method for dielectric breakdown voltage and dielectric strength of solid electrical insulating materials at commercial power frequencies, ASTM, West Conshohocken, PA, 2004, pp. 1-13.
10. Verhaart H. F. A., Tom J., Verhage A. J. L. and Vos C. S. - Avalanches near solid insulators, Proceeding of the 5th Int. Symp. on High Voltage Engineering, Germany, 1987, paper 13.01.
11. Krile J. T., Neuber A. A., Dickens J. C. and Krompholz H. G. - Physics of dielectric surface breakdown at atmospheric pressure, Proceeding of the 14th IEEE International Pulsed Power Conference, USA, 2003, pp. 285-288.
12. Krile J. T., Neuber A. A., Dickens J. C. and Krompholz H. G. - DC flashover of a dielectric surface in atmospheric conditions, IEEE Trans. Plasma Sci. **32** (5) (2004) 1828-1834. https://doi.org/10.1109/TPS.2004.835483.
13. Mitchinson, P. M., Lewin, P. L. and Strawbridge, B. D. - Tracking and surface discharge at the oil-pressboard interface, IEEE Electr. Insul. Mag. **26** (2) (2010) 35-41. https://doi.org/10.1109/MEI.2010.5482553.
14. Mo Y. K., Lee O., Kim J., Bang S., Kang J. O., Lee H., Choi S. and Kang H. - Surface discharge characteristics of gfrp in GN_2 and LN_2 for designing a superconducting coil system, IEEE Trans. Applied Superconductivity **26** (4) (2016) 1-4. https://doi.org/10.1109/TASC.2016.2541624.
15. Chiba M. and Nitta T. - Surface spark-over voltage on solid insulator in sub-cooled liquid nitrogen, IEEE Trans. Applied Superconductivity **15** (2) (2005) 1743-1746. https://doi.org/10.1109/TASC.2005.849271.
16. Frayssines P. E., Lesaint O., Bonifaci N., Denat A. and Devaux F. - Prebreakdown and breakdown phenomena under uniform field in liquid nitrogen and comparison with mineral oil, IEEE Trans. on Dielectr. Electr. Insul. **10** (6) (2003) 970-976. https://doi.org/10.1109/TDEI.2003.1255774.